

Original orthorhombic tetrahedral-trigonal hybrid allotropes

C_n ($n= 8, 10, 12, 14$) with *ethene*-like and *propadiene*-like units:

Crystal chemistry and first principles.

Samir F. Matar

Lebanese German University (LGU), CMMS, Sahel Alma, Lebanon

 <https://orcid.org/0000-0001-5419-358X>

Abstract.

*Original carbon allotropes, orthorhombic C_8 , C_{10} , C_{12} and C_{14} presenting mixed sp^2/sp^3 carbon hybridizations exhibiting $C=C$ ethene-like and $C=C=C$ propadiene-like embedded units are proposed from crystal chemistry and calculations within the quantum density functional theory DFT. The carbon allotropes with topologies related with **jeb**, **mog**, as well as new topologies, show alternating tetrahedral and trigonal carbon stacking along the a -orthorhombic direction (vertical) close to but different from “isoglitter”. The carbon allotropes (C_8 , C_{10} , C_{12} , C_{14}) were shown to be cohesive and stable both mechanically (elastic properties) and dynamically (phonons), with calculated Vickers hardness (H_V) magnitudes ranging between 25 GPa and 52 GPa, the latter magnitude assigned to C_{12} possessing the largest number of tetrahedral versus trigonal stacking. High phonon frequencies $\omega \sim 50$ THz were attributed to stretching mode of $C=C$ (in C_8 and C_{12}) and $C=C=C$ (in C_{10} and C_{14}) components with good agreement with experiment for Raman molecular $C=C$ intense stretching mode. Magnitudes of $\omega \sim 40$ THz were proposed as signatures of $C-C$ simple bonds in the tetrahedra. The electronic band structure and electronic density of states DOS shown exemplarily for C_8 point to metallic-like behavior assigned mainly to the itinerant role of trigonal carbon π -electrons.*

Keywords: DFT, mixed hybridization, carbon, phonons, hardness

Introduction

The challenging field of carbon research has a particular position among scientists, especially with diamond recognized as the hardest material. Beside this aristo-type, there is an ongoing search for original carbon allotropes that achieve similar mechanical and thermal properties with help provided by modern materials research programs based on evolutionary crystallography such as CALYPSO [1]. A library of such original mainly artificial allotropes is devoted to store the structures (SACADA) [2], classified by different topologies that are identified using TopCryst program [3]. For instance, diamond is labeled as **dia**, and its rare hexagonal form *Lonsdaleite*, is labeled along with similar or derived allotropes by **lon**.

The tetrahedral C(sp³) hybridization makes diamond a perfectly covalent system with large electronic band gap of ~5 eV. However, a change to semi-conductive and metallic behaviors useful for applications in electronics, can be induced by self-doping with C(sp²). Back in 1994, Bucknum et al. [4] proposed tetragonal C₆ allotrope called “glitter”, i.e. shining and conductive. The crystal system was built ad hoc from 1,4-cyclohexadienoid units. Topology wise, glitter C₆ is called **tfi** and classified in SACADA data base under No. 95. Another arrangement of cyclohexadiene-type units was identified by us recently based on diamond-like template structure with an original tetragonal C₆ we called “neoglitter” characterized by ultra-hardness with metallic behavior and identified with **tfa** topology [5].

In 2012, a mixed sp³/sp² carbon system was also identified for orthorhombic C₈ called “isoglitter” with **jeb** topology (actually **jeb,bbe-3,4-Cmmm** as referred to by TopCryst) and SACADA No. 105 classification [6]. The structure shown in Fig. 1a exhibits along the ‘a’ orthorhombic direction (vertical axis) a succession of one trigonal layer -white central spheres- with ∠C-C-C angle of 120° corresponding to C(sp²) hybridization, then followed by a tetrahedral layer with C(sp³) (brown central sphere) with perfect C(sp³) tetrahedral ∠C-C-C angle of 109.47°, and lastly 2 trigonal layers (white central spheres). The relationship with organic chemistry with the use of 1,4-cyclohexadienoid cycle stands well but it also reproduces an ethene-like >C=C< unit with the white spheres aligned vertically (connected here with terminal carbons) whilst ethene or ethylene molecule has the formula C₂H₄. Another similar structure regarding the double tetrahedra stacks is **mog** C₆ (SACADA No. 96) shown in Fig. 1b. However, a major difference appears with the connection of the two tetrahedral layers by squares of carbon atoms as shown with the polyhedral projection; such configuration is deemed less stable as shown later.

Figure 1c shows our novel orthorhombic C_8 having **jeb** topology with another connection of two tetrahedral arrays connected through trigonal C=C (white spheres). The structure close to “isoglitter” is hence called by us “metaglitter”.

Preliminary investigation of the relative ground state cohesive energies led to $E_{\text{coh./atom}}$ (metaglitter C_8) = -2.20 eV versus $E_{\text{coh./atom}}$ (isoglitter C_8) = -2.15 eV, and $E_{\text{coh./atom}}$ (**mog**- C_6) = -1.01 eV, which is then the least cohesive/stable.

The purpose of the present work is to delve further in the context of carbon allotropes with mixed hybridizations, by proposing novel orthorhombic allotropes with diene $>C=C<$ units as well as larger systems embedding propadiene-like $>C=C=C<$ units (propadiene molecule: C_3H_4).

All studied systems, rationalized through crystal chemistry approaches were quantitatively investigated within the quantum mechanics Density Functional Theory (DFT) [7,8], specifically their cohesiveness, electronic, mechanical, and dynamic stabilities as well as the electronic properties in relation with the presence of C=C / C=C=C units.

1- Computational methodology

For the devised stoichiometries the identifications of the ground state structures characterized by energy minima (and derived cohesive energies) and the prediction of their mechanical and dynamical properties called for calculations with methods based on the DFT. Herein, we used the Vienna Ab initio Simulation Package (VASP) code [9,10] and the projector augmented wave (PAW) method [10,11] for the atomic potentials. Exchange correlation (XC) effects were considered using the generalized gradient functional approximation (GGA) [12]. The relaxation of the atoms onto the ground state structures was performed with the conjugate gradient algorithm according to Press *et al.* [13]. The Blöchl tetrahedron method [14] was used for geometry optimization and energies. The Brillouin-zone (BZ) integrals were approximated by a special \mathbf{k} -point sampling according to Monkhorst and Pack [15]. Structural parameters were optimized until atomic forces were below 0.02 eV/Å and all stress components were $< 0.003 \text{ eV/Å}^3$. The calculations were converged at an energy cutoff of 400 eV for the plane-wave basis set in terms of the \mathbf{k} -point integration in the reciprocal space from $k_x(6) \times k_y(6) \times k_z(6)$ up to $k_x(12) \times k_y(12) \times k_z(12)$ for the final convergence and relaxation to zero strains. In the post-processing of the ground state electronic structures, the charge density projections were operated on the lattice sites. The mechanical stability and hardness were obtained from the calculations of the elastic constants. The treatment of the results was done thanks to ELATE

[16] online tool devoted to the analysis of the elastic tensors providing the bulk B and shear G modules along different averaging methods; Voigt's method was used herein [17]. For the calculation of the Vickers hardness a semi-empirical model based on elastic properties was used [18]. The dynamic stabilities were confirmed from the phonon positive magnitudes. The corresponding phonon band structures were obtained from a high resolution of the Brillouin Zone according to Togo *et al.* [19]. The electronic band structures were obtained using the all-electron DFT-based ASW method [20] and the GGA XC functional [12]. The VESTA (Visualization for Electronic and Structural Analysis) program [21] was used to visualize the crystal structures and charge densities.

2- Crystal chemistry rationale

2.1. C₈ “metagitter” allotrope

Besides the above liminary investigations reporting on the comparative cohesive energy magnitudes between three carbon allotropes favoring presently proposed “metagitter” C₈, preliminary mechanical stability criteria obtained with similar conditions of calculations showed all-positive elastic constants (*vide infra*) versus presence of negative elastic constants in “isogitter”. The “metagitter” C₈ allotrope crystal parameters obtained after full geometry optimization to the ground state structure are given in Table 1a (the structure was already shown in Fig. 1c). The atoms are distributed over two four-fold Wyckoff positions, namely (4g) brown spheres and (4h) with white spheres of the base-centered orthorhombic space group *Cmmm* No. 65. The largest lattice constant is a_{orth} , so that the vertical orientation of the structure is along this parameter. The shortest interatomic distance of 1.34 Å is between the two trigonal carbon (white) atoms, equivalent to the magnitude admitted for C=C in ethene. This value is intermediate between $d(\text{C}-\text{C}) = 1.54 \text{ \AA}$ for C(sp³) as in diamond, and triple bond $d(\text{C}\equiv\text{C}) = 1.20 \text{ \AA}$ as in ethyne or acetylene (C₂H₂) with C(sp¹) hybridization. The other distances are slightly below and above $d(\text{C}-\text{C})$. The angles show the tetrahedral configuration signature with $\angle\text{C1-C1-C1} = 109.48^\circ$, while noting that the angle $\angle\text{C2-C1-C2} = 114.54^\circ$ is smaller but close to trigonal magnitude of 120°.

2.1. Addressing the problematic of stacking tetrahedra.

The larger cohesive energy of metagitter C₈ versus the two other allotropes above could be assigned to the larger number of tetrahedral layers connected by trigonal carbons. The interplay between the stacking and connection of the tetrahedra and the resulting cohesive energy having

been addressed, it was relevant to examine the effect of creating double layer-stacking of tetrahedra within the base-centered orthorhombic carbon sublattices by going to higher stoichiometry.

Orthorhombic C_{12} was subsequently obtained by additional tetrahedral carbon positioned at a second four-fold Wyckoff position ($4h$) versus C_8 . The geometry optimization led to a stable system with energy $E_{\text{coh./atom}}(C_{12}) = -2.26$ eV (Table 1 2nd column), i.e. more stable than C_8 , thus confirming the hypothesis that a larger content of tetrahedral stacks as shown in Fig. 1d, is responsible for the higher cohesive energy and the system is closer to diamond cohesive energy which amounts to -2.47 eV/atom. Concomitantly the density of C_{12} increases versus C_8 despite the larger volume, letting confirm the role played by additional tetrahedral carbon in the structure densification. The distance between trigonal carbon (white spheres along vertical direction) amounts to 1.34 Å, as in C_8 . The angles are of two types: trigonal for $\angle C2-C2-C3=122.99^\circ$ (close to 120°) and tetrahedral with $\angle C1-C3-C1=109.97^\circ$ and $\angle C1-C1-C3=109.15^\circ$. Different topology was identified for C_{12} with the label: **3,4,4T154**.

2.3. Embedding $C=C=C$ propadiene-like units: base centered orthorhombic C_{10} and C_{14} allotropes.

Following the effect brought by additional tetrahedra leading to enhanced stability, it was relevant to check the effect of inserting in C_8 an additional trigonal carbon occupying the two-fold Wyckoff ($2c$) $0, \frac{1}{2}, \frac{1}{2}$ position in space group $Cmmm$, i.e., the center of the plane orthogonal to the vertical direction (orthorhombic a), i.e. a face center position as shown with the red spheres in Fig. 2a. After full geometry optimization C_{10} was obtained with structure parameters shown in Table 2, 1st column; the topology is **jeb**. Expectedly a larger volume versus C_8 was found due to the larger interatomic distances. Also, the angles show closer magnitudes to trigonal hybridization with 115.44° and 122.28° versus one tetrahedral-like angle $\angle C2-C1-C1$ of 109.16° . The additional carbon shown in red forms with the two-neighboring white (trigonal) atoms a $>C=C=C<$ propadiene linear entity with terminal carbons instead of hydrogen in the propadiene molecule C_3H_4 . The cohesive energy is found with lower magnitude than pristine C_8 with $E_{\text{coh./atom}}(C_{10}) = -1.81$ eV. Then, increasing the trigonal character of the structure plays opposite role versus tetrahedral character. The density decreases due to the larger volume of C_{10} on one hand and to the introduction of more trigonal carbon, on the other hand.

Lastly, C_{14} was also devised based on C_{12} , with converged ground state described in 2nd column of Table 2 and depicted in Figure 2b exhibiting the propadiene units as in C_{10} . The

extension of the lattice versus C_{12} leads to a larger cohesive energy of $E_{\text{coh.}/\text{atom}}(C_{14}) = -2.02$ eV, versus $E_{\text{coh.}/\text{atom}}(C_{12}) = -1.81$ eV. Crystal analyses showed that the two allotropes presented 3,4,4T154 topology, different from **jeb**.

3- Projection of the charge density.

In view of the structure description with the presence of C=C and C=C=C units based on organic chemistry-like reasoning; further illustration of chemistry \leftrightarrow crystal structure relationship is needed. It can be provided qualitatively by the charge density projections shown with yellow volumes around atoms displayed in Figure 3. C_8 (Fig. 3a) and C_{12} (Fig. 3b) show the trigonal C=C with red high charge concentration at the intersection with the plane. Tricarbon containing C_{10} (Fig. 3c) and C_{14} (Fig. 3d) show the C=C=C propadiene entities with large concentration observed at the plane crossing in Fig. 3c representing C_{10} . Such concentrations of charge densities are signatures of C=C and C=C=C since less yellow volumes intensities are observed for C-C simple bonds forming the tetrahedral network.

4- Physical properties: results and discussions

3.1 Mechanical properties from the elastic constants

The analysis of the mechanical properties was carried out with the calculation of the elastic properties by operating finite distortions of the lattice. The system is then fully described by the bulk (B) and the shear (G) moduli obtained by averaging the elastic constants. The calculated sets of elastic constants C_{ij} (i and j corresponding to directions) are given in Table 2.

All C_{ij} values are positive letting expect mechanically stable systems. C_8 and C_{12} have the largest C_{ij} values whereas derived C_{10} and C_{14} present intermediate values. Such magnitudes are translated by the bulk B_V and shear G_V modules obtained from ELATE program [16] devoted to the analysis of the elastic tensors. The last columns of Table 2 provide the obtained B_V and G_V (V subscript designated adopting Voigt averaging method (ref. [17]) showing magnitudes following the trends observed for C_{ij} .

Subsequently the hardness according to Vickers (H_V) was predicted using the model of Chen et. al. [18]:

$$H_V = 0.92 (G/B)^{1.137} G^{0.708}$$

with H_V possessing the same unit as G_V , and B_V , i.e., GPa.

In this equation G/B is called the Pugh ratio [22] that allows distinguishing ductile behavior ($G_V/B_V < 1$) from brittle behavior ($G_V/B_V > 1$). All allotropes present $G_V/B_V < 1$ with the highest values observed for C_{12} close to 1 ($G_V/B_V = 0.91$). C_{12} that contains the largest amount of four tetrahedral stacks is found on the verge of brittleness, whereas C_8 has $G_V/B_V = 0.82$ with two tetrahedral layers within the orthorhombic cell. On the other side, C_{10} and C_{14} characterized by large trigonal C content have $G_V/B_V = 0.75$, lower than in C_8 and C_{12} with a rather ductile behavior. The last column of Table 2 reflects these observations with the highest magnitude of Vickers hardness $H_V(C_{12}) = 52$ GPa pointing to super-hard behavior, larger than $H_V(C_8) = 43$ GPa on one hand and $H_V(C_{10}) = 32$ GPa, $H_V(C_{14}) = 36$ GPa showing close magnitudes, on the other hand letting assign them average hardness behaviors. Note however that $H_V(C_{12}) = 52$ GPa remains far below diamond's which amounts to ~ 95 GPa cf. [5] and therein cited works.

The mechanical results agree well with the crystal chemistry description above reporting on the role played by tetrahedral stacking.

3.2 Dynamic and thermodynamic properties from the phonons

An important criterion of phase dynamic stability is obtained from the phonon's properties. Phonons defined as quanta of vibrations have their energy quantized thanks to the Planck constant 'h' used in its reduced form \hbar ($\hbar = h/2\pi$). The phonons energy is given by $E = \hbar\omega$ where ω is the frequency. Figure 4 depicts in four panels the phonons band structures of the four allotropes along the major lines of the orthorhombic Brillouin zone (x -axis). The frequency along the y -axis is expressed in units of Tera-Hertz (THz, with $1 \text{ THz} = 33 \text{ cm}^{-1}$). There are $3N-3$ optical modes found at higher energy than three acoustic modes that start from zero energy ($\omega = 0$) at the Γ point that defines the center of the Brillouin Zone, up to a few Terahertz. They correspond to the lattice rigid translation modes of the crystal (two transverse and one longitudinal). The remaining bands correspond to the optic modes. All phonon frequencies are found positive letting confirm the stability of the announced allotropes from the point of view of dynamic stability. The highest frequencies in all panels are close to 50 THz, equivalent to 1650 cm^{-1} . This magnitude is exactly within the range of C=C vibrations with a strong signal, i.e., $1625\text{--}1680 \text{ cm}^{-1}$ in the molecular state as listed in the web-available "RAMAN Band Correlation Table". The second highest vibration is found with bands around 40 THz, signature of the tetrahedral carbon [23].

The thermodynamic properties of the new phases were calculated from the phonon frequencies using the statistical thermodynamic approach [24] on a high-precision sampling

mesh in the orthorhombic Brillouin zone. The temperature dependencies of the heat capacity at constant volume (C_v) are shown in Figure 5 for one and two tetrahedral stack allotrope C_8 and C_{12} in comparison with experimental C_v data for diamond by Victor [25]. The calculated curves of both C_8 and C_{12} follow closely the evolution of diamond experimental points but the curves are systematically above the experimental points. Note that C_{12} which contains larger number of tetrahedra versus C_8 presents a curve closer to diamond. The interpretation relies here too on the fact the diamond is uniquely made of tetrahedra, whereas C_{12} and C_8 possess trigonal and tetrahedral carbons.

3-3 Electronic band structures and density of states DOS

Is so far that the main feature in all four allotropes is the concomitant presence of tetragonal and trigonal carbon sites, we consider the electronic structure of C_8 as their illustrative representative in Figure 6. The band structure in Fig. 6a shows the bands developing along the main directions of the orthorhombic BZ. The zero energy along the y-axis is considered with respect to the Fermi level E_F crossed by finite bands, and there's no separation between the valence band VB and the conduction band CB at E_F . C_8 has then a metallic character. One can observe that without the dispersing of these bands crossing E_F at R and Y points, C_8 would be semi-conducting or small-gap insulator. Assigning these bands can be better assessed from the site projected density of states DOS in Fig. 6b where the energy axis is now horizontal, and the DOS are expressed in eV^{-1} . Tetrahedral carbon (C1) DOS are shown in purple lines whereas trigonal carbon (C2) DOS are represented with blue-green lines. Within the VB, from -22 eV up to E_F the DOS of the two carbon sites show resemblance in the major part, whence the bonding between the two carbon sub-structures C1 and C2. s-like states are found up to -15 eV, with s(C1) showing more localized character (σ electrons) than smeared s(C2) with delocalized π electrons. Most importantly one observed vanishingly small magnitude of C1 DOS which behave diamond $C(sp^3)$ -like at E_F versus C2 DOS which behave $C(sp^2)$ -like. Therefore, C2 is responsible of the band crossing at E_F and of the metallic character.

5- Conclusion

The main purpose of this paper was to highlight the effects on the physical properties of the concomitant presence of $C(sp^3)$ -like and $C(sp^2)$ -like carbons in a series of hybrid carbon allotropes. Orthorhombic C_8 , and C_{12} exhibit C=C ethene-like subunits whereas C_{10} and C_{14}

present C=C=C (propadiene)-like subunits, all connecting tetrahedral stacks of layers. The proposed allotropes from crystal chemistry were quantitatively investigated with calculations of energies and energy-based quantities as the elastic and dynamic and electrons structures. All allotropes were shown to be cohesive and stable both mechanically (elastic properties) and dynamically (phonons), with calculated Vickers hardness (HV) magnitudes ranging between 25 GPa and 52 GPa; the latter large magnitude was assigned to C₁₂ containing the largest number of tetrahedral stackings. The highest phonon frequencies $\omega \sim 50$ THz were attributed to the Raman stretching mode of diene C=C units while lower magnitudes $\omega \sim 40$ THz were proposed as signatures of C-C bonds in the tetrahedra as in diamond. In C₈ and C₁₂ allotropes the temperature evolution of the specific heat C_v follows diamond's experimental discrete points while being at higher values. The electronic band structure points to metallic-like behavior assigned mainly to the itinerant role of trigonal carbon delocalized π -electrons.

REFERENCES

- [1] S. Zhang, J. He, Z. Zhao, D. Yu, Y. Tian, Discovery of superhard materials via CALYPSO methodology. *Chinese Phys. B* **28** (2019) 106104.
- [2] SACADA (Samara Carbon Allotrope Database). www.sacada.info
- [3] V. A. Blatov, A.P. Shevchenko, et al.. Applied topological analysis of crystal structures with the program package ToposPro, *Cryst. Growth Des.*, **14** (2014), 3576–3586.
- [4] M.J. Bucknum, R. Hoffmann. A hypothetical dense 3,4-connected carbon net and related B₂C and CN₂ nets built from 1,4-cyclohexadienoid units. *J. Am. Chem. Soc.* **116** (1994) 11456-11464.
- [5] S.F. Matar, V.L. Solozhenko. Novel ultrahard sp²/sp³ hybrid carbon allotrope from crystal chemistry and first principles: Body-centered tetragonal C₆ ('neoglitter'). *Diamond & Related Mater.* **133** (2023) 109747.
- [6] M.J. Bucknum; E.A. Castro, B. Wen. Isoglitter, *J. Math. Chem.* **50** (2012) 2281.
- [7] P. Hohenberg, W. Kohn. Inhomogeneous electron gas. *Phys. Rev. B* **136** (1964) 864-871.
- [8] W. Kohn, L.J. Sham. Self-consistent equations including exchange and correlation effects. *Phys. Rev. A* **140** (1965) 1133-1138.
- [9] G. Kresse, J. Furthmüller. Efficient iterative schemes for ab initio total-energy calculations using a plane-wave basis set. *Phys. Rev. B* **54** (1996) 11169.
- [10] G. Kresse, J. Joubert. From ultrasoft pseudopotentials to the projector augmented wave. *Phys. Rev. B* **59** (1999) 1758-1775.
- [11] P.E. Blöchl, Projector augmented wave method. *Phys. Rev. B* **50** (1994) 17953-17979.
- [12] J. Perdew, K. Burke, M. Ernzerhof, The Generalized Gradient Approximation made simple. *Phys. Rev. Lett.* **77** (1996) 3865-3868.
- [13] W.H. Press, B.P. Flannery, S.A. Teukolsky, W.T. Vetterling, *Numerical Recipes*, 2nd ed. Cambridge University Press: New York, USA, 1986.
- [14] P.E. Blöchl, O. Jepsen, O.K. Anderson, Improved tetrahedron method for Brillouin-zone integrations. *Phys. Rev. B* **49** (1994) 16223-16233.
- [15] H.J. Monkhorst, J.D. Pack. Special k-points for Brillouin Zone integration. *Phys. Rev. B* **13** (1976) 5188-5192.
- [16] R. Gaillac, P. Pullumbi, F.X. Coudert. ELATE: an open-source online application for analysis and visualization of elastic tensors. *J. Phys.: Condens. Matter* **28** (2016) 275201.
- [17] W. Voigt, Über die Beziehung zwischen den beiden Elasticitätsconstanten isotroper Körper. *Annal. Phys.* **274** (1889) 573-587.
- [18] X.Q. Chen; H. Niu, D. Li, Y. Li. Modeling hardness of polycrystalline materials and bulk metallic glasses. *Intermetallics* **19** (2011) 1275-1281.

- [19] A. Togo, I. Tanaka, First principles phonon calculations in materials science, *Scr. Mater.* **108** (2015) 1-5.
- [20] V. Eyert, The Augmented Spherical Wave Method, Lect. Notes Phys. 849 (Springer, Berlin Heidelberg 2013).
- [21] K. Momma, F. Izumi. VESTA3 for three-dimensional visualization of crystal, volumetric and morphology data. *J. Appl. Crystallogr.* **44** (2011) 1272-1276.
- [22] D.B. Miracle. Generalization of intrinsic ductile-to-brittle criteria by Pugh and Pettifor for materials with a cubic crystal structure. *Scientific Reports* **11** (2021) 4531.
- [23] R.S. Krishnan, Raman spectrum of diamond, *Nature* **155** (1945) 171
- [24] M.T. Dove, Introduction to lattice dynamics. Cambridge University Press: New York, USA, 1993.
- [25] A.C. Victor, Heat capacity of diamond at high temperatures. *J. Chem. Phys.* **36** (1962) 1903.

Table 1. Crystal structure parameters of the orthorhombic carbon allotropes.

a) C₈ (**jeb**) and C₁₂ (**3,4,4T154**).

| <i>Cmmm</i> No. 65 | C ₈ | C ₁₂ |
|---|--|--|
| <i>a</i> , | 7.8026 | 11.3788 |
| <i>b</i> , Å | 2.6786 | 2.5179 |
| <i>c</i> , Å | 2.5054 | 2.6231 |
| <i>V</i> _{cell} , Å ³ | 52.36 | 75.14 |
| Density g/cm ³ | 3.053 | 3.185 |
| Distances <i>d-d</i> - Å | d(C2-C2)= 1.34 d(C2-C1)= 1.49 d(C1-C1)= 1.64 | d(C3-C3)=1.34 d(C1-C1)=1.534 d(C3-C1)=1.60 |
| Angles (deg.) | ∠C2-C1-C2= 114.54° ∠C2-C1-C1= 108.19° ∠C1-C1-C1= 109.48° | ∠C2-C2-C3=122.99° ∠C1-C3-C1=109.97° ∠C1-C1-C3=109.15° |
| Atomic position | C1 (4g) 0.8107, ½, 0 C2 (4h) 0.4139, 0, ½ | C1 (4g) 0.7886, ½, 0 C2 (4h) 0.0589, 0, ½ C3 (4h) 0.1307, ½, ½ |
| E(coh.)/at. eV | -2.20 | -2.26 |

b) C₁₀ and C₁₄ (**3,4,4T154** topology)

| <i>Cmmm</i> No. 65 | C ₁₀ (jeb) | C ₁₄ |
|---|---|---|
| <i>a</i> , | 10.6745 | 14.1952 |
| <i>b</i> , Å | 2.4833 | 2.4932 |
| <i>c</i> , Å | 2.6429 | 2.5732 |
| <i>V</i> _{cell} , Å ³ | 70.675 | 91.07 |
| Density g/cm ³ | 2.845 | 3.066 |
| Distances <i>d-d</i> - Å | d(C2-C3)=1.35 d(C2-C1)=1.56 d(C1-C1)=1.57 | d(C2-C4)=1.34 d(C2-C3)=1.51 d(C1-C2)=1.58 |
| Angles (deg.) | ∠C2-C1-C2=115.44° ∠C2-C1-C1=109.16° ∠C1-C2-C3=122.28° | ∠C3-C2-C4=124.13 ∠C1-C1-C3=109.63° ∠C2-C3-C1=109.04° |
| Atomic position | C1 (4g) 0.7955, ½, 0 C2 (4h) 0.3734, 0, ½ C3 (2c) 0, ½, ½ | C1 (4g) 0.7811, ½, 0 C2 (4h) 0.0946, 0, ½ C3 (4h) 0.1541, ½, ½ C4 (2d) 0, 0, ½ |
| E(coh.)/at. eV | -1.81 | -2.02 |

E(C) = -6.6 eV. E_{diamond} (coh.)/at. = -2.49 eV.; E(N)=-6.8 eV

Table 2. Elastic constants, bulk B_V , and shear G_V moduli and hardness H_V in GPa units.

| | C_{11}/C_{22} | C_{12} | C_{13}/C_{23} | C_{33} | C_{44} | C_{55} | C_{66} | B_V | G_V | H_V |
|----------|-----------------|----------|-----------------|----------|----------|----------|----------|-------|-------|-------|
| C_8 | 1136/575 | 35 | 169/4 | 1173 | 31 | 120 | 510 | 375 | 308 | 43 |
| C_{10} | 1272/846 | 114 | 76/68 | 289 | 340 | 112 | 46 | 325 | 243 | 32 |
| C_{12} | 1092/1144 | 149 | 77/18 | 678 | 526 | 213 | 98 | 378 | 345 | 52 |
| C_{14} | 1159/943 | 162 | 95/110 | 673 | 366 | 181 | 95 | 390 | 288 | 36 |

FIGURES

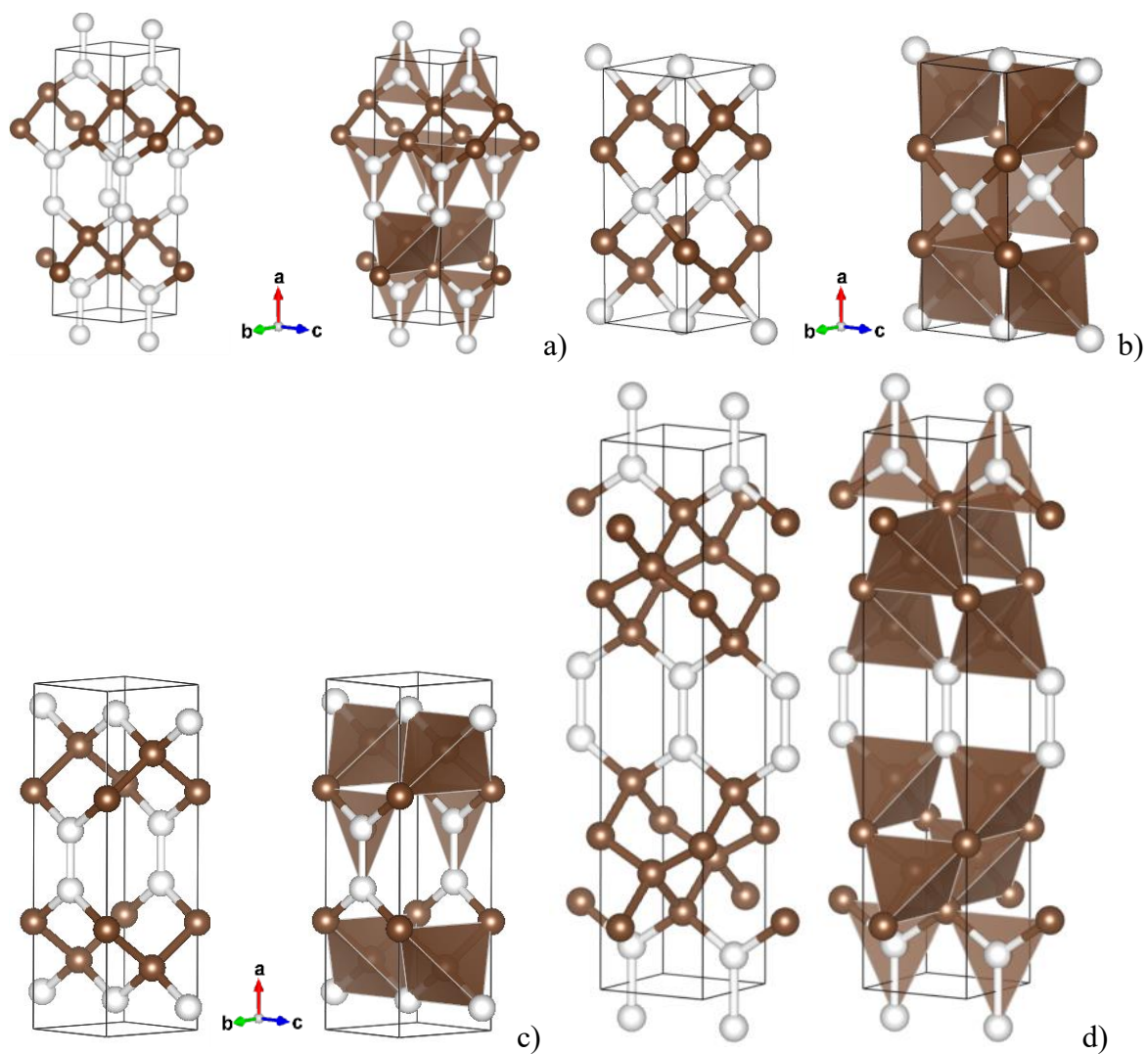


Figure 1. Sketches of the orthorhombic crystal structures with ball-and-stick (left) and polyhedral (right) representations: a) C_8 isoglitter (**jeb** topology) SACADA No.105, b) C_6 (**mog** topology) SACADA No. 96, c) C_8 *present work*, d) C_{12} *present work*. Brown and white spheres correspond to tetrahedral and trigonal different carbon sites (cf. Table 1).

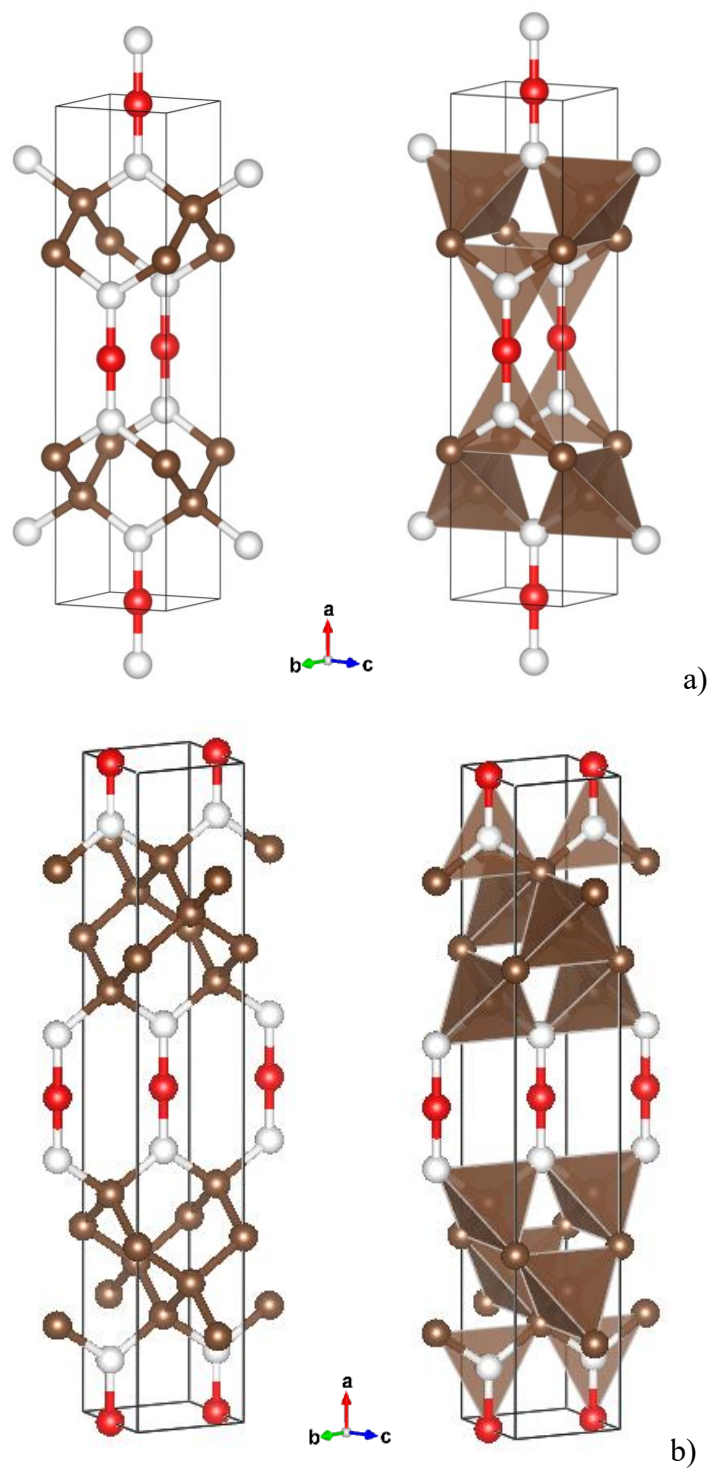


Figure 2. Sketches of the orthorhombic crystal structures with ball-and-stick (left) and polyhedral (right) representations: a) C_{10} , b) C_{14} . Brown, white and red spheres correspond to carbon on different sites (cf. Table 1).

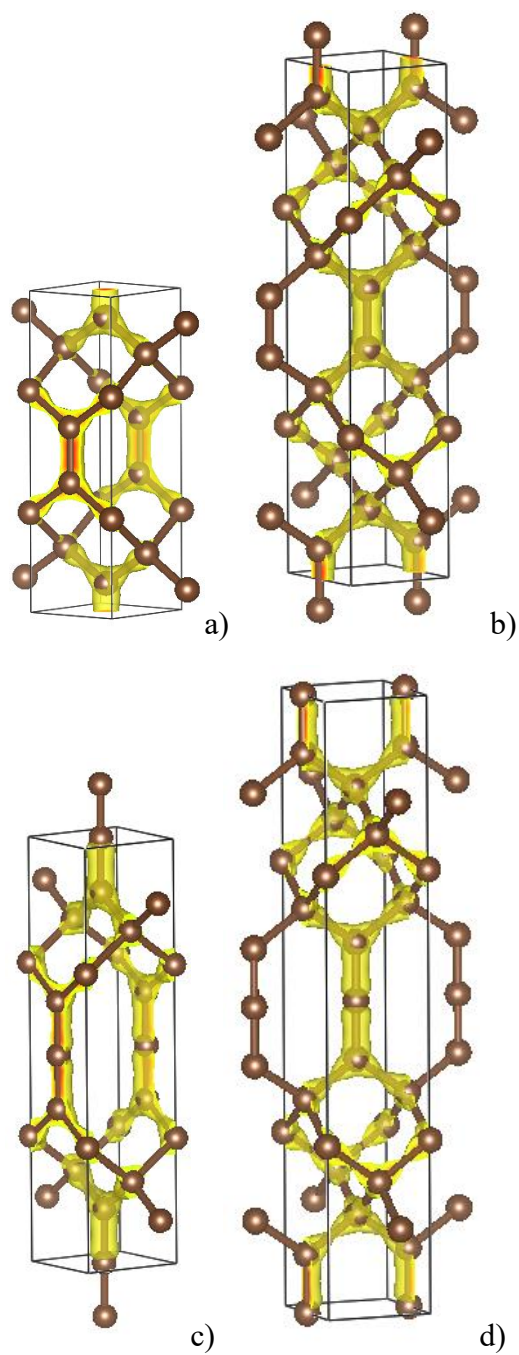


Figure 3. Charge density projections (yellow volumes) of a) C_8 , and b) C_{12} , showing $C=C$ - like diene entities, and c) C_{10} , and d) C_{14} with propadiene $C=C=C$ -like entities. The vertical direction is along the orthorhombic a lattice parameter.

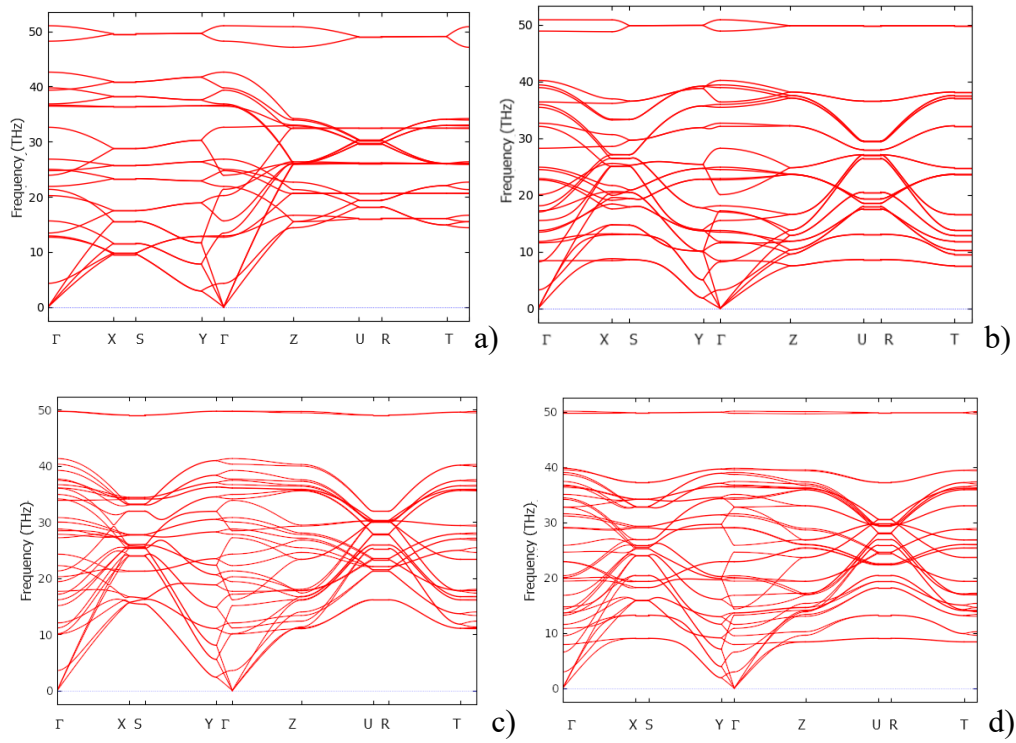


Figure 4. Phonons band structures along the major lines of the orthorhombic Brillouin zone (x-axis). Frequency along the y-axis is expressed in units of Terahertz (THz). a) C_8 , b) C_{10} , c) C_{12} , and d) C_{14} .

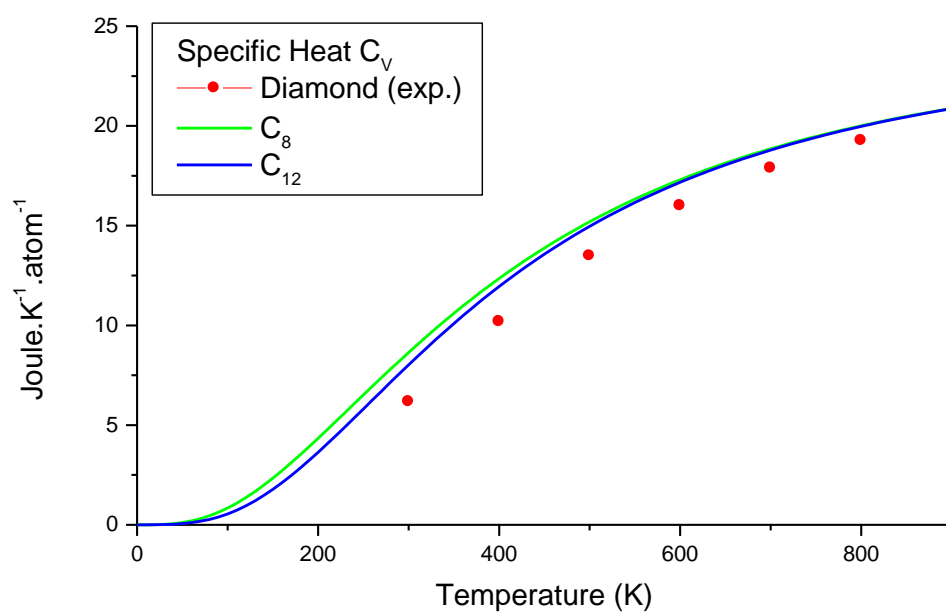


Figure 5. Thermal properties with the calculated specific heat C_V of C_8 and C_{12} ; the experimental values of diamond from literature are shown with red dots.

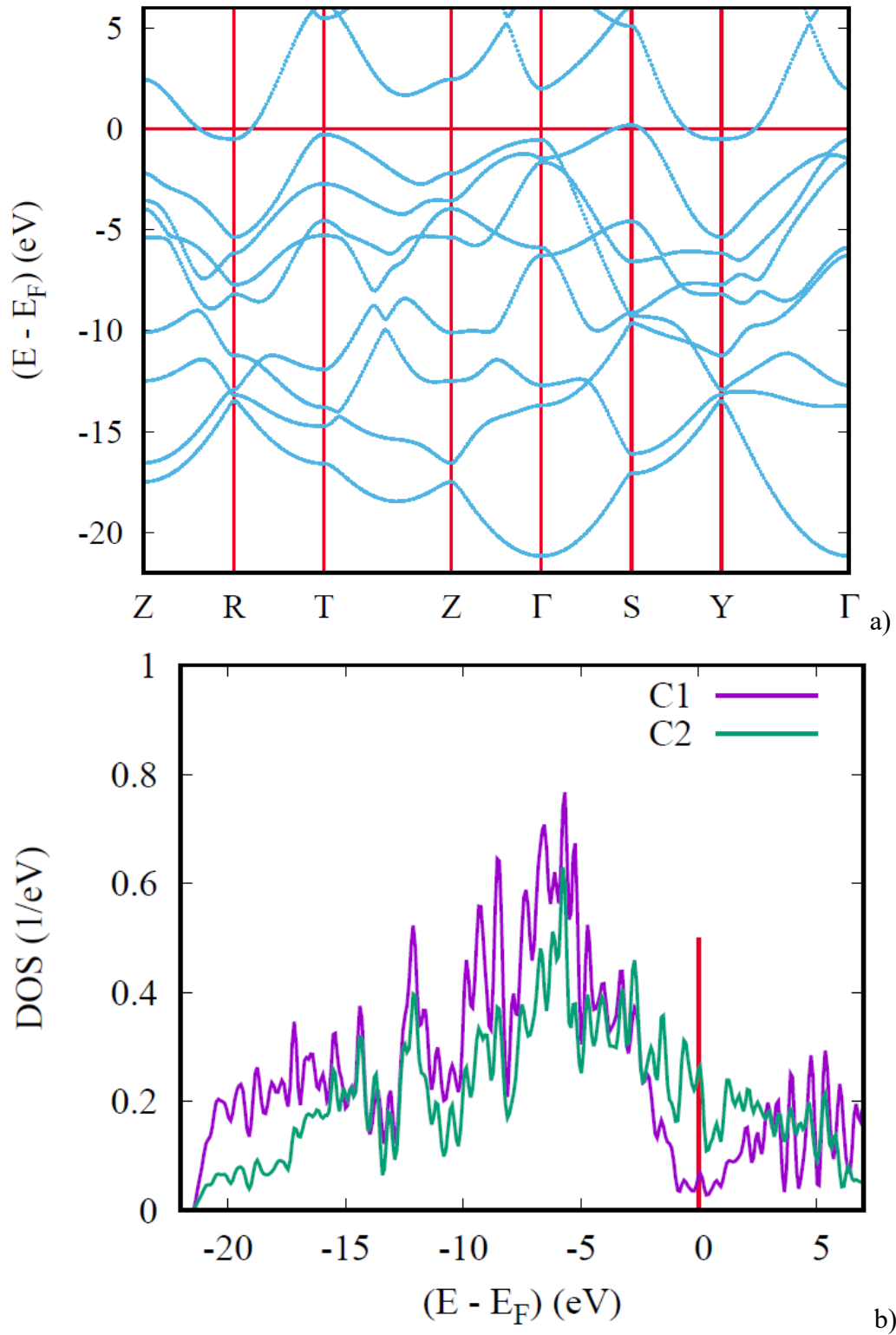


Figure 6. C₈. Electronic band structure along major lines of the orthorhombic Brillouin zone along x -axis (a), and site projected density of states (b). Energy is referenced with respect to the Fermi level (E_F) and expressed in units of electron-Volts (eV).